RSC Advances

PAPER

View Article Online
View Journal | View Issue

Check for updates

Cite this: *RSC Adv.*, 2023, **13**, 28753

Enhancing acid orange II degradation in ozonation processes with $CaFe_2O_4$ nanoparticles as a heterogeneous catalyst

Huu Tap Van,[ab] Van Hung Hoang,*[cd] Thi Cuc Luu,[d] Thuy Linh Vi,[b] Luong Thi Quynh Nga,[e] Gio Serafin Ivan Jimenez Marcaida[f] and Truong-Tho Pham[gh]

This study used $CaFe_2O_4$ nanoparticles as a catalyst for ozonation processes to degrade Acid Orange II (AOII) in aqueous solution. The study compared heterogeneous catalytic ozonation ($CaFe_2O_4/O_3$) with ozone treatment alone (O_3) at different pH values (3–11), catalyst dosages (0.25–2.0 g L^{-1}), and initial AOII concentrations (100–500 mg L^{-1}). The O_3 alone and $CaFe_2O_4/O_3$ systems nearly completely removed AOII's color. In the first 5 min, O_3 alone had a color removal efficiency of 75.66%, rising to 92% in 10 min, whereas the $CaFe_2O_4/O_3$ system had 81.49%, 94%, and 98% after 5, 10, and 20 min, respectively. The O_3 and $CaFe_2O_4/O_3$ systems degrade TOC most efficiently at pH 9 and better with 1.0 g per L $CaFe_2O_4$. TOC removal effectiveness reduced from 85% to 62% when the initial AOII concentration increased from 100 to 500 mg L^{-1}. The study of degradation kinetics reveals a pseudo-first-order reaction mechanism significantly as the solution pH increased from 3 to 9. Compared to the O_3 alone system, the $CaFe_2O_4/O_3$ system has higher k values. At pH 9, the k value for the $CaFe_2O_4/O_3$ system is 1.83 times higher than that of the O_3 alone system. Moreover, increasing AOII concentration from 100 mg L^{-1} to 500 mg L^{-1} subsequently caused a decline in the k values. The experimental data match pseudo-first-order kinetics, as shown by R^2 values of 0.95–0.99. AOII degradation involves absorption, ozone activation, and reactive species production based on the existence of CaO and FeO in the $CaFe_2O_4$ nanocatalyst. This catalyst can be effectively recycled multiple times.

Received 10th July 2023
Accepted 15th September 2023

DOI: 10.1039/d3ra04553f

rsc.li/rsc-advances

Open Access Article. Published on 02 October 2023. Downloaded on 2/9/2026 11:33:56 AM.
This article is licensed under a Creative Commons Attribution-NonCommercial 3.0 Unported Licence.

Introduction

Along with numerous industrial pollutants, textile dyes are highly toxic and potentially carcinogenic.[1] Dye pollution is a significant environmental problem that can negatively impact human health and ecosystems. Discharging highly toxic and possibly carcinogenic textile dyes into water bodies causes water pollution.[1–3] The textile industry significantly contributes to water pollution because of its high water consumption and discharge of coloring materials.[2] Dye contamination can inhibit microalgae growth and disrupt trophic interactions.[3] Synthetic dyes in the textile industry, dyeing and printing industry, tannery and paint industries, paper and pulp industry, and cosmetic and human health industries can have catastrophic effects on human health and the environment.[2]

It has been determined that azo dyes are deleterious to aquatic organisms and carcinogenic and mutagenic for humans. As a result, it is of the utmost importance to develop efficient techniques for removing azo dyes from the effluent before discharge into the environment. Due to stringent environmental regulations, the significance of dye removal technology has increased. Physical adsorption, chemical coagulation, advanced oxidation, membrane filtration, adsorption, photocatalysis, and biologically based technology have all been investigated for dye removal.[4–6] The technique of film-supported catalysts attracts considerable interest.[7] Physical adsorption is generally regarded as an efficient technique for rapidly reducing the concentration of dissolved dyes, and activated carbon is the most commonly used adsorbent for dye removal.[8] Dye removal technologies based on biopolymers can potentially become viable alternatives for the remediation of industrial dye effluents and contaminated water bodies.[8] Using

[a]Center for Advanced Technology Development, Thai Nguyen University, Tan Thinh Ward, Thai Nguyen City, Vietnam
[b]Faculty of Natural Resources and Environment, TNU – University of Sciences, Tan Thinh Ward, Thai Nguyen City, Vietnam
[c]Thai Nguyen University, Tan Thinh Ward, Thai Nguyen City, Vietnam. E-mail: hoangvanhung@tnu.edu.vn
[d]Faculty of Agriculture and Forestry, TNU – Lao Cai Campus, Lao Cai City, Vietnam
[e]Department of Infectious Diseases, Faculty of Sub-Specialties, Thai Nguyen University of Medicine and Pharmacy (TNUMP), No. 284, Luong Ngoc Quyen Street, Thai Nguyen City, Vietnam
[f]Department of Environmental Science and Management, Advanced Education Program, TNU – University Agriculture and Forestry (TUAF), Quyet Thang Ward, Thai Nguyen City, Vietnam
[g]Laboratory of Magnetism and Magnetic Materials, Science and Technology Advanced Institute, Van Lang University, Ho Chi Minh City, Vietnam
[h]Faculty of Applied Technology, School of Technology, Van Lang University, Ho Chi Minh City, Vietnam

© 2023 The Author(s). Published by the Royal Society of Chemistry

Open Access Article. Published on 02 October 2023. Downloaded on 2/9/2026 11:33:56 AM. This article is licensed under a Creative Commons Attribution-NonCommercial 3.0 Unported Licence.

agro/industrial waste residues for dye adsorption has been highlighted as a possible alternative material for dye removal.[4] Membrane technology incorporating an electric field has demonstrated good dye removal performance and is believed to have a promising future.[5] Nonetheless, most of these methods are limited by the production of toxic sludge and high operational and maintenance costs.[6] Advanced oxidation technology is one of the most effective methods for dye removal among these technologies.[9]

In the advanced oxidation processes (AOPs), ozonation is one of the techniques used to degrade azo dyes.[10–12] Due to their complex structure, azo dyes resist ozone, light, biodegradation, and other environmental conditions.[13] Nanocatalysts have been used to degrade azo dyes, including acid orange II, in catalytic ozonation. The application of nanocatalysts can significantly boost the degradation and mineralization of dyes. Fe_3O_4/multi-walled carbon nanotubes have been used to catalyze the ozonation of *p*-hydroxybenzoic acid.[14] In another study, using iron oxide as a catalyst in ozonation to degrade sunset yellow dye was proposed.[15] Nanocatalysts of the spinel-type $ZnAl_2O_4$ have also been used in catalytic ozonation for wastewater treatment.[16] The nano-ZnO/perlite catalyst has been used for catalytic ozonation of azo dyes, significantly improving the dye's mineralization.[17] In addition, Fe–Ni bimetallic nanoparticles have been utilized as a catalyst for the degradation of orange G dye by ozone.[18] In a recent study conducted by Meng *et al.* (2022),[19] an assessment was carried out regarding the advancements and obstacles encountered in the electro- and photocatalytic oxidation of hydroxymethylfurfural derived from biomass. This oxidation process aims to convert hydroxymethylfurfural into valuable chemicals, notably 2,5-formylfuran (DFF) and 2,5-furandicarboxylic acid (FDCA). Solid catalytic materials with bifunctional properties were employed in the sequential conversion of biomass into biofuels and associated chemicals.[20] Also, a Mn/Mg/Ce ternary ozone catalyst was used to degrade printing and dyeing wastewater.[21] It has been discovered that Ag and Au nanoparticles decorated on chitosan-functionalized graphene oxide exhibit excellent catalytic activity for reducing aromatic nitroarenes and degradation of azo dyes.[22] Under ambient conditions, magnetically recyclable $CoFe_2O_4$/ZnO nanocatalysts have been utilized for the efficient catalytic degradation of acid blue 113.[23] For the photocatalytic degradation of methyl orange, methylene blue, and rhodamine B, the AgCl nanocatalyst synthesized from its bulk material in the ionic liquid trihexyl(tetradecyl)phosphonium chloride has been used.[24] These studies reveal the potential of nanocatalysts for the ozone-based treatment of wastewater containing azo dyes. Therefore, ozone catalytic oxidation improves dyeing wastewater treatment after catalyst addition. Consequently, nanocatalysts enhance the efficiency of ozone degradation of azo dyes.

$CaFe_2O_4$ nanoparticles are a novel catalyst for the ozone degradation of Acid Orange II (AOII). While other nanocatalysts, such as Fe_3O_4/multi-walled carbon nanotubes and $CoFe_2O_4$/ZnO, have been studied for the degradation of azo dyes using ozone, the use of $CaFe_2O_4$ nanoparticles for this purpose is uncommon. The mechanism of the catalytic ozonation process with the $CaFe_2O_4$ nanocatalyst to enhance the production of hydroxyl radicals, which are responsible for the degradation of the dye, was also investigated in this study. Consequently, using the $CaFe_2O_4$ nanocatalyst as a catalyst for the ozone degradation of acid orange II is a promising strategy that merits further investigation.

This research aims to synthesize $CaFe_2O_4$ nanocatalysts and examine their potential as a catalyst for the ozone-mediated degradation of AOII in aqueous solutions. This study aims to determine the effect of solution pH and nanoparticle amount on the degradation of AOII. In addition, the effect of initial AOII concentration on the degradation process will be investigated. In addition, the study will determine the reaction rate constant to evaluate the degradation process's efficacy. By examining these factors, this study aims to shed light on the usefulness of $CaFe_2O_4$ nanoparticles as a catalyst for the degradation of AOII. The findings will ultimately contribute to developing effective and sustainable methods for treating wastewater containing dyes.

Materials and methods

Chemicals

Acid Orange II (AOII) dye, with the formula $26H_{17}ClN_7Na_3O_{10}S_3$ (Fig. 1), was imported from Tianjin De Sheng Wang Chemical Trade Co., Ltd., China, and utilized without further purification. $CaCO_3$, Fe_2O_3, H_2SO_4, and NaOH chemicals were obtained from Merck & Co., Inc. To prepare a laboratory-synthesized AOII dye solution, 1.0 g of AOII was dissolved in 1 L of deionized water to obtain a 1000 mg L^{-1} concentration. The stock AOII solution was diluted with distilled water to produce synthetic wastewater samples with AOII concentrations ranging from 100 to 500 mg L^{-1}. Ozone (O_3) was produced to remove AOII using the NextOzone ozone generator model Next 10P, which has a maximal ozone production capacity of 10 g O_3 per h. The ozone was introduced through the bottom inlet of the reactor.

Synthesis of catalyst materials

Synthesis of $CaFe_2O_4$ nanoparticles. $CaFe_2O_4$ nanoparticles were prepared through a two-step fabrication method consisting of a conventional solid-state reaction process and a high-energy ball milling process. The synthesis process involved high-purity $CaCO_3$ and Fe_2O_3 oxides as starting materials. First, the polycrystalline $CaFe_2O_4$ sample was obtained by subjecting the mixture of $CaCO_3$ and Fe_2O_3 to a solid-state reaction at 1000 °C. The resulting sample was then annealed for 2 h.

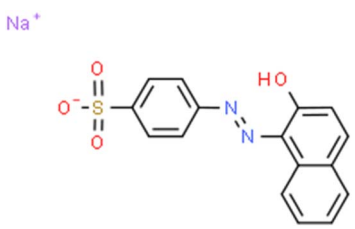

Fig. 1 Chemical structure of AOII.

© 2023 The Author(s). Published by the Royal Society of Chemistry

Open Access Article. Published on 02 October 2023. Downloaded on 2/9/2026 11:33:56 AM.
This article is licensed under a Creative Commons Attribution-NonCommercial 3.0 Unported Licence.

Subsequently, the annealed sample was pelletized and sintered in air at a temperature of 1200 °C to obtain $CaFe_2O_4$ nanoparticles.[25] This fabrication method ensures the formation of ultra-fine particles of $CaFe_2O_4$, which is crucial for their enhanced catalytic properties.

Experimental setup

The ozone treatment system employed a tubular borosilicate glass reactor with a volume of 1.2 L (height = 450 mm, inner diameter = 60 mm).[26] The reactor had a gas inlet, outlet ports, and sampling accessories. To investigate the effects of AOII solution pH and $CaFe_2O_4$ nanoparticle dosage (in fluidized status), $CaFe_2O_4$ nanoparticles were introduced into the reactor along with 500 mL of AOII solution at the desired concentration. Ozone was generated from pure oxygen using an ozone generator (NextOzone 20P, International Ozone Generator Company, Vietnam). The ozone production rate was maintained at 15 mL min^{-1}, and regulated by a flow meter, and ozone was introduced into the reactor from the bottom through a diffuser. The reactor, containing 500 mL of AOII solution, ensured uniform distribution of $CaFe_2O_4$ nanoparticles throughout the solution using a porous glass diffuser. Each ozonation cycle lasted for 5 min, with a total treatment time of 50 min.

Analytical methods

The degree of mineralization of AOII following degradation was assessed by measuring the concentration of total organic carbon (TOC) using a TOC analyzer (Multi N/C 3100, Germany). Additionally, the color change was analyzed using a double-beam UV/vis spectrophotometer (Shimadzu, Model Z2000, Japan) at a wavelength of 483 nm.

The pore volume and surface area of $CaFe_2O_4$ nanoparticles were determined using the Brunauer–Emmet–Teller (BET) method on an SA 3000 instrument (Coulter, USA). The morphology of the $CaFe_2O_4$ nanoparticles was observed using a transmission electron microscope (SEM) equipped with TEM, JEOL JEM-2100 Plus, Hillsboro, USA. The X-ray diffraction (XRD) pattern of the $CaFe_2O_4$ nanoparticles was recorded using a Siemens D5005 X-ray diffractometer with Cu Kα radiation (λ = 1.5417 Å).

Results and discussion

Characteristics of $CaFe_2O_4$ nanoparticles

$CaFe_2O_4$ nanoparticles as a catalyst for the degradation of acid orange II dye with ozone have the following characteristics: average pore volume of 0.011 cm^3 g^{-1}, average surface area of 379 m^2 g^{-1}, and average particle size of 11.63 nm. The TEM analysis of $CaFe_2O_4$ nanoparticles from Fig. 2a reveals their rough surface texture and a variety of structures with varying sizes. These structures have an uneven distribution and a propensity to clump together. Amorphous $CaFe_2O_4$ nanoparticles are distinguished by their irregular shapes and lack of uniformity. The average diameter of $CaFe_2O_4$ particles ranges from 500 to 1000 nm, and they form clusters of varying sizes. The SEM analysis reveals a broad size distribution within these clustered structures, whose dimensions are relatively homogeneous. While maintaining their anisotropic shape, the particles exhibit interconnected irregular and porous structures. Individual particle sizes range from 70 to 300 nm, while the maximum length of the anisotropic nanostructures is 650 nm. Remarkably, the particles exhibit remarkable interconnectivity and cohesion while retaining an open structure, which enhances their capacity for efficient substance absorption. These porous structures provide favorable conditions for adsorption processes in aqueous environments.

The EDS analysis of $CaFe_2O_4$ nanoparticles (Fig. 2b) verifies the presence of oxygen (O), calcium (Ca), and iron (Fe) elements, which account for 46.10%, 13.53.3%, and 40.30%, respectively, of the total weight. These elements have respective atomic weight percentages of 73.10%, 8.56%, and 18.34%. EDS analysis provides information about the percentage composition of chemical elements present in the material. In the case of the $CaFe_2O_4$ nanocatalyst, EDS results reveal the presence of calcium (Ca), iron (Fe), and oxygen (O). These elements play a crucial role in the ozone degradation process of azo dyes. Therefore, this demonstrates that $CaFe_2O_4$ is a potential catalyst for ozonation to degrade various azo dyes. Therefore, the nano $CaFe_2O_4$ nanoparticles can be utilized as a catalyst for the ozonation of AOII.

X-ray diffraction (XRD) analysis was used to examine the phase composition of the $CaFe_2O_4$ nanocatalyst material. Fig. 2c demonstrates the XRD analysis results of the $CaFe_2O_4$ nanocatalyst. The X-ray diffraction pattern provides insight into the nanoparticle crystallinity of the $CaFe_2O_4$ nanocatalyst. The nano $CaFe_2O_4$ nanocatalyst phase can be seen in Fig. 2c with major and low-intensity peaks. The crystalline structure of $CaFe_2O_4$ nanoparticles can be deduced using the widely employed XRD measurement technique. The (302) and (210) planes at 2θ angles of 33.6° and 35.41°, respectively, account for the former peak. Additionally, notable peaks (102) at 2θ = 19.25°, (113) at 2θ = 40.39°, (311) at 2θ = 42.1°, (214) at 2θ = 49.71°, and (512) at 2θ = 61.23° have been observed. These XRD patterns of the $CaFe_2O_4$ nanocatalyst display multiple peaks, each corresponding to a distinct crystallographic plane within the crystal structure. The XRD results of $CaFe_2O_4$ from this study are similar to the findings reported by Alhassan *et al.*,[27] showing that the planes (102), (202), (302), (210), (113), (311), (214), and (512) correspond to the 2θ angles of 19.2°, 25.7°, 33.6°, 35.6°, 40.4°, 42.8°, 49.6°, and 61.4°, respectively. Understanding materials' physical and chemical characteristics using the data from XRD measurements is useful for creating new applications in sensing, energy storage, and catalysis.

The FTIR spectrum of $CaFe_2O_4$ nanoparticles exhibits various absorption peaks corresponding to distinct vibrational modes of the chemical bonds inherent in the nanoparticles.[28] A broad absorption peak is evident within the 3402 to 3851 cm^{-1} range, indicative of the O–H stretching mode.[29] Peaks at 1081 and 1635 cm^{-1} signify the elongation of C–O bonds.[30] A peak at 1779 cm^{-1} suggests the existence of C=O functional groups, potentially resulting from the establishment of hydrogen bonds between water groups and silanols. The absorption peaks at 2849 and 2916 cm^{-1} exhibit lower intensity, implying the

Open Access Article. Published on 02 October 2023. Downloaded on 2/9/2026 11:33:56 AM.
This article is licensed under a Creative Commons Attribution-NonCommercial 3.0 Unported Licence.

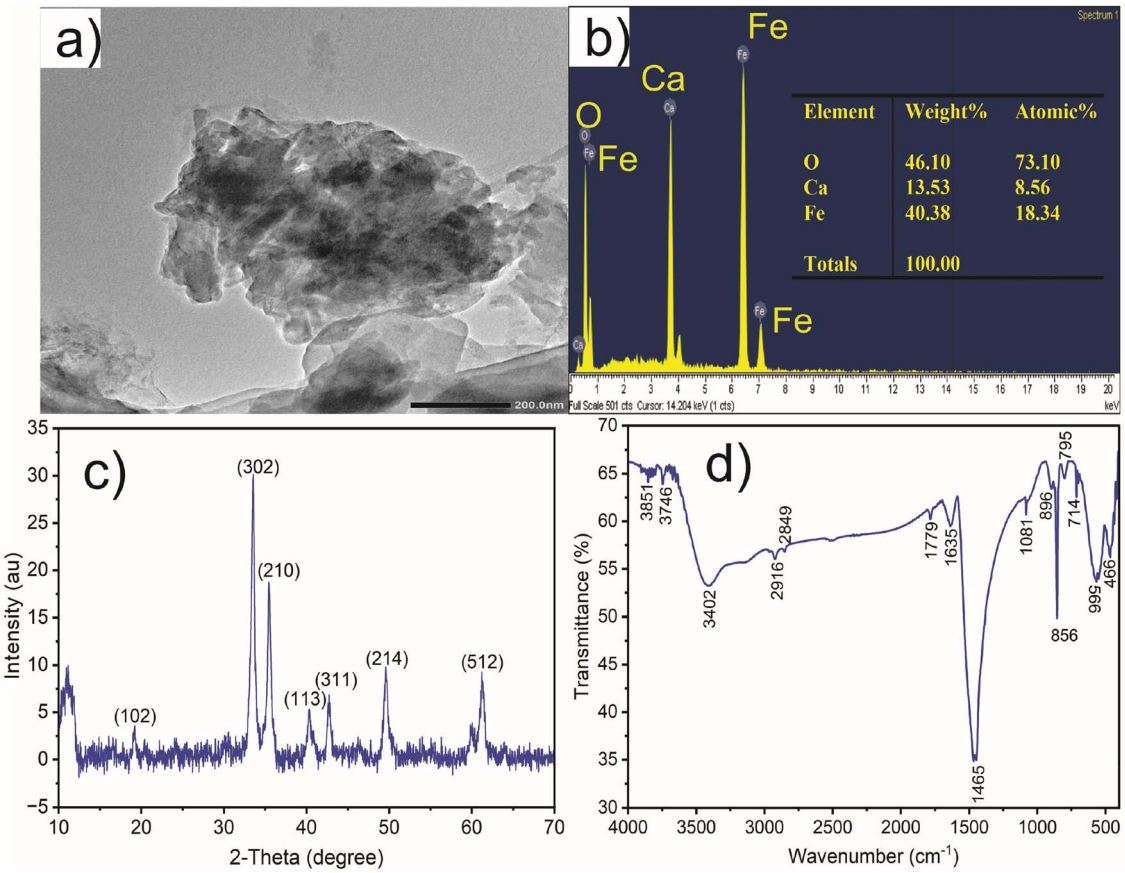

Fig. 2 TEM (a), EDX (b), XRD (c) and FTIR (d) graph of $CaFe_2O_4$ nanoparticles.

reduced stretching of C–H bonds. The FTIR spectrum offers insights into the calcium (Ca) and iron (Fe) bonds within the $CaFe_2O_4$ nanoparticles. Peaks at wavelengths of 466 and 566 cm^{-1} correspond to the Ca–O and Fe–O bonds, respectively.[31] Moreover, peaks at 856 and 896 cm^{-1} emerge from bending Fe–O–H bonds, while peaks at 714 and 759 cm^{-1} arise from the elongation of Fe–O bonds.[28]

The effect of solution pH on AOII degradation

The details offered make it clear how pH affects the concentration and rate of disintegration of AOII during the ozonation process. This dramatically impacts how quickly azo dyes react and how well they degrade. The pH of the solution directly influences the rate at which hydroxyl radicals are produced and the availability of the iron catalyst inside the reactor.

Experiments were carried out to determine the effect of solution pH on the decolorization and total organic carbon (TOC) degradation effectiveness of AOII. The pH ranged from 3 to 11, with variations. The catalyst dosage was 1.0 g L^{-1}, the starting concentration of AOII was fixed at 200 mg L^{-1}, and the contact times for AOII were 0–50 min, respectively (Fig. 3).

According to the data shown in Fig. 3, both ozone alone (O_3 alone) and $CaFe_2O_4$ nanocatalytic ozone ($CaFe_2O_4/O_3$) systems demonstrate distinct patterns in the decolorization and total organic carbon (TOC) degradation of AOII at various pH levels. From pH 3 to pH 9, the decolorization and TOC degradation rates of AOII typically decrease, with a minor fall at pH 11 (Fig. 3a and c).

For both O_3 alone and $CaFe_2O_4/O_3$ systems, the decolorization rate of AOII advanced quickly, reaching approximately 100% in a short reaction time of 25 min. However, the efficiency of TOC decomposition varied. When the pH rose from 3 to 9, the efficiency of O_3 alone ranged between 49% and 59%. It slightly decreased to 57% after 40 min of reaction time (Fig. 3b). The TOC degradation efficiency in the $CaFe_2O_4/O_3$ system varied from 58% to 75% when the solution pH increased from 3 to 9. It dropped to 72% when the pH was further raised to 11 within the same 40 min reaction period (Fig. 3d). Therefore, the findings shown in Fig. 3 reveal that both O_3 alone and $CaFe_2O_4/O_3$ systems achieve their maximum AOII degradation efficiency under alkaline conditions (pH 9), with the $CaFe_2O_4/O_3$ system demonstrating a higher efficiency than O_3 alone by a margin of 10% to 16%. It is noteworthy that, compared to ozone alone (O_3 alone), the $CaFe_2O_4/O_3$ system's usage of $CaFe_2O_4$ nanocatalytic ozone exhibits the most effective AOII degradation. It is essential to note that pH levels over 11 did not improve AOII treatment efficiency in this investigation compared to pH 9.

Acid orange II can be directly attacked by ozone through electrophilic reactions in an acidic environment.[32] Peroxynitrous acid attacks acid orange II using a radical cage solvent

© 2023 The Author(s). Published by the Royal Society of Chemistry

Open Access Article. Published on 02 October 2023. Downloaded on 2/9/2026 11:33:56 AM.
This article is licensed under a Creative Commons Attribution-NonCommercial 3.0 Unported Licence.

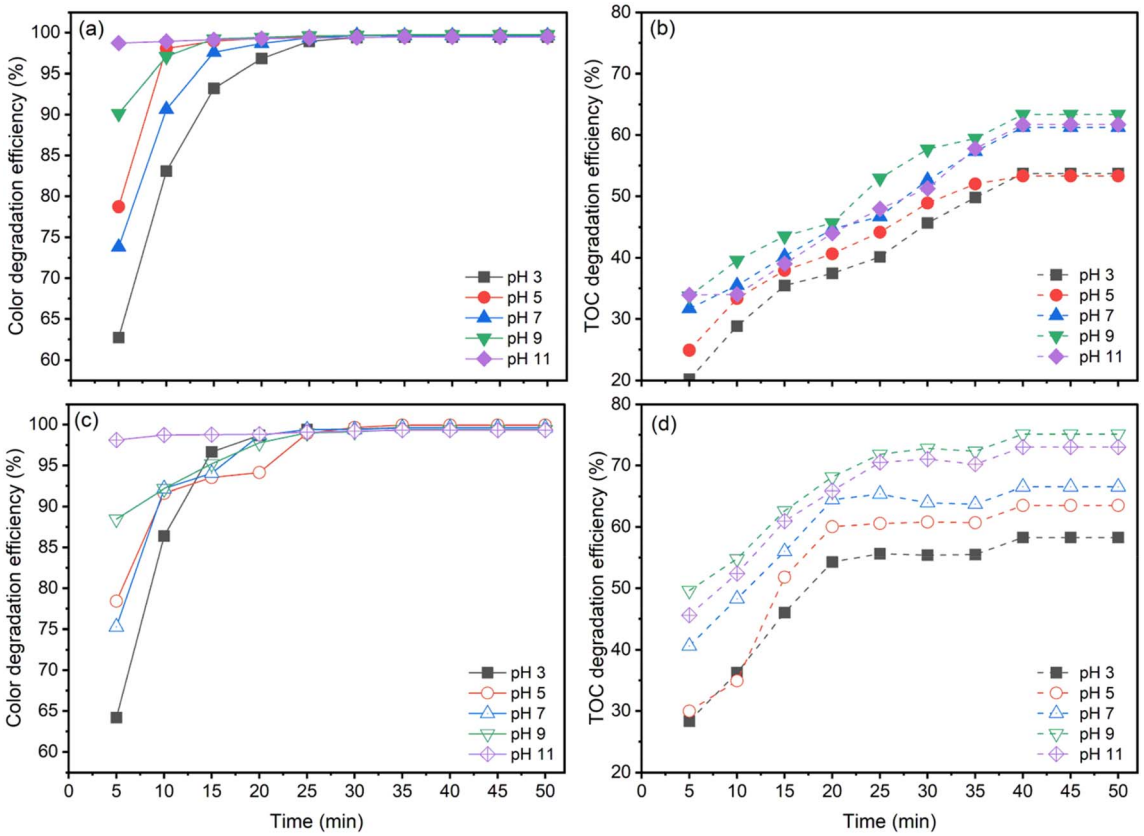

Fig. 3 Color and TOC degradation efficiency for AOII by ozone alone (a and b) and $CaFe_2O_4$ nanocatalytic ozone (c and d) at various solution pH values. Conditions: [AOII] = 200 mg L^{-1}, catalyst dosage = 1.0 g, contact time = 50 min, and reaction temperature = 25 ± 2 °C.

during this chemical process. Previous research[33] has examined the oxidation of orange II with ozone and H_2O_2/O_3 oxidation systems. In addition, orange II has been observed to undergo decolorization under various conditions.[34] The production of isocyanates *via* the nucleophilic or electrophilic reaction of ozone with isonitriles has also been reported[35] as a reaction involving ozone. In previous literature,[36] the electrophilic attack of ozone on aromatic bonds has also been discussed.

According to the well-established Criegee mechanism of ozonation, the dominant mechanism for the oxidation of acid orange II by O_3 molecules[37] will be direct ozonation. However, due to the formation of aldehydes and carboxylic acids that do not react continuously with ozone, the reaction rate is sluggish and selective, resulting in incomplete degradation of organic matter.[38] The reaction between hydroxide ions (–OH) and ozone (O_3) results in the formation of superoxide (O_2^-) and hydroperoxide ($HO_2^{\cdot}$) radicals, according to several investigations.[39–41] The hydroxide ions catalyze ozone decomposition, and the concentration of hydroperoxide and superoxide radicals increases with increasing pH. Ozone then continuously reacts with superoxide radicals to produce highly reactive hydroxyl ($^{\cdot}OH$) radicals, effectively oxidizing organic and inorganic compounds in water. Several studies[39,40] corroborate that an increase in ozone degradation rates occurs as pH increases. Due to ozone's lower oxidation potential than hydroxyl radicals, direct oxidation by ozone is slower than radical oxidation.[42]

In one study, however, pH levels greater than 11 did not enhance the treatment efficiency of AOII compared to pH 9.[43] The study examined the decomposition of AOII using ozone and hydrogen peroxide (H_2O_2) in a batch reactor under varying pH conditions. After 60 min of treatment, the highest degradation efficiency was observed at pH 9, with a rate of 98.5%. At pH levels greater than 11, however, the degradation efficiency dropped to 92.5% after 60 min of treatment. The study suggested that the decrease in degradation efficiency at high pH levels may be attributable to the formation of hydroxide ions, which can compete with AOII for ozone and H_2O_2, thereby decreasing the concentration of reactive species available for AOII degradation. According to additional studies, the optimal pH range for the degradation of various organic compounds using ozone and H_2O_2 is 7–9.[44–46]

The $CaFe_2O_4$ nanocatalyst is a variety of catalyst that has demonstrated great promise for enhancing the removal of AOII from aqueous solutions by catalytic ozonation. In catalytic ozonation systems, using the $CaFe_2O_4$ nanocatalyst as a heterogeneous catalyst has increased the generation of $^{\cdot}OH$ radicals. The primary mechanism underlying the activation of catalytic ozonation is that the catalyst accelerates the production of hydroxyl radicals $^{\cdot}OH$, which result from the decomposition of ozone by the catalyst. This increases the oxidation potential, thereby accelerating the degradation of AOII. Due to its ability to support substantially as an ozonation catalyst

Open Access Article. Published on 02 October 2023. Downloaded on 2/9/2026 11:33:56 AM. This article is licensed under a Creative Commons Attribution-NonCommercial 3.0 Unported Licence.

($CaFe_2O_4/O_3$) and enhance the removal of AOII from aqueous solutions, the $CaFe_2O_4$ nanocatalyst is considered the most intriguing catalyst. Nanocatalysts were discovered to increase the production of $^{\bullet}OH$ radicals in catalytic ozonation systems.[47] Another study mentioned using a manganese catalyst in heterogeneous catalytic ozonation, indicating that hydroxyl radicals play a significant role in the oxidation process.[48] Shokrollahzadeh *et al.*[17] also reported that adding a nano-ZnO/perlite nanocatalyst increased the degradation rate during the catalytic ozonation of an azo dye. Overall, these references demonstrated that nanocatalysts improved the performance of catalytic ozonation systems by producing hydroxyl radicals.

The comparison between heterogeneous catalytic ozonation ($CaFe_2O_4/O_3$) and O_3 alone revealed that catalytic ozonation systems were more effective at TOC degradation than non-catalytic ozonation systems (O_3 alone). Catalytic ozonation is a technology for the non-selective degradation of organic matter in water utilizing active free radicals produced by ozone degradation.[49] The AOII degradation by $CaFe_2O_4/O_3$ and O_3 alone was more efficacious as the solution pH rose from 3 to 9. Notably, the AOII degradation efficiency, as measured by the removal of TOC, was lower than that of AOII decolorization. This disparity results from AOII's distinct contributions to color and TOC. The main source of color is dyed with complete chromophores, and the destruction of the dye chromophore through the cleavage of the –N=N– group in AOII is more accessible than the degradation of AOII into CO_2, H_2O, and other byproducts. The color disappeared when the molecular structure of AOII was broken down by the direct or indirect reaction with O_3, either through $^{\bullet}OH$ radicals. Still, the complete conversion of organic matter into CO_2 and H_2O had not yet occurred. As a result, the efficiency of TOC degradation was lower than the decolorization rate. Ozonation resulted in a greater decolorization than TOC degradation efficiency.[50] In phosphate- and bicarbonate-buffered solutions, the comparison between conventional ozonation and heterogeneous catalytic ozonation processes revealed that catalytic ozonation systems exhibited superior decolorization and TOC degradation efficiency compared to non-catalytic ozonation systems.[51]

The effect of $CaFe_2O_4$ nanocatalyst mass on AOII degradation

Experiments were conducted at pH 9 with an ozone generation rate of 3.038 g h^{-1} for both O_3 alone and $CaFe_2O_4/O_3$ systems. The study examined the decolorization and degradation of AOII *via* color and TOC elimination and varying the dosage of the $CaFe_2O_4$ nanocatalyst (0.25 to 2.0 g L^{-1}) at an initial AOII concentration of 200 mg L^{-1}, solution pH of 9 and contact time of 0–50 min. The results are shown in Fig. 4.

Fig. 4a illustrates the color removal efficiency of AOII *via* ozone catalysis under various conditions: ozone alone and $CaFe_2O_4/O_3$ with variable amounts of $CaFe_2O_4$ nanocatalyst. Both processes degraded AOII, resulting in rapid color reduction within five to ten minutes of the reaction. When considering ozone alone, the color removal efficiency for a 5 min contact time began at 75.66%. With extended contact times, the efficiency increased progressively, reaching 92% after 10 min of contact. The color removal efficacy remained constant at 92% until the 50 minute period. In the $CaFe_2O_4/O_3$ system, adding 0.25 g per L $CaFe_2O_4$ nanocatalyst increased the color removal efficiency to 81.49% after 5 min of reaction, 94% after 10 to 20 min and 98% after 50 min. The color removal efficiency gradually improved as the dosage of the $CaFe_2O_4$ nanocatalyst increased from 0.5 g L^{-1} to 2 g L^{-1}. After 20 min of reaction with the $CaFe_2O_4$ nanocatalyst ranging between 0.5 g L^{-1} and 2 g L^{-1}, the color removal efficiency reached a maximum of 98%. The swift progression of AOII decolorization in the O_3 and $CaFe_2O_4/O_3$ systems arises from the catalytic breakdown of dye molecules.[52] When AOII exists in its initial colored form, its molecular structure is disrupted, causing an instant loss of color. Particularly in the O_3 system, O_3 acted as a potent oxidizing agent, directly breaking down the structure of dye molecules and swiftly diminishing AOII color within a 10 minute period. The presence of $CaFe_2O_4$ nanoparticles in the $CaFe_2O_4/O_3$ system enhanced decolorization further. These nanoparticles served as catalysts, promoting the degradation process of dye molecules by O_3, aided by their high adsorption capacity, enabling effective interaction between dye molecules and O_3, thereby accelerating the decolorization process. The synergistic strength between O_3 and $CaFe_2O_4$ nanoparticles even accelerates the rate beyond that of O_3 alone, manifested by a higher decolorization rate in the $CaFe_2O_4/O_3$ system due to increased adsorption surface area, intensifying the catalytic degradation efficiency.

Fig. 4b displays the influence of $CaFe_2O_4$ nanocatalyst dosage on the TOC removal efficiency of AOII using O_3 alone and $CaFe_2O_4/O_3$ systems over time. For a contact time of 5 min, the TOC removal efficacy for O_3 alone began at 34%. The efficiency progressively increased as the contact time increased, reaching 58% after 30 min. After 40 min and 50 min of reaction, the efficiency increased insignificantly. Regarding the $CaFe_2O_4/O_3$ systems, when 0.25 g per L $CaFe_2O_4$ nanocatalyst was added, the TOC removal efficiency began at 38% after 5 min and increased steadily to 61% after 25 min, without further improvement with extended reaction times. Upon increasing the amount of $CaFe_2O_4$ nanocatalyst from 0.25 g L^{-1} to 1.0 g L^{-1}, the efficiency of TOC treatment exhibited an ascending trend, reaching a maximum of 83.38% after 40 min of reaction, and then remained stable for the next 50 min. Increasing the $CaFe_2O_4$ nanocatalyst dosage to 1.5 g L^{-1} and 2.0 g L^{-1} leads to a minor decrease in efficiency. The results demonstrate that adding the $CaFe_2O_4$ nanocatalyst improves the efficiency of TOC elimination compared to O_3 alone. The $CaFe_2O_4$ nanocatalyst at a dosage of 1.0 g L^{-1} provides the most outstanding efficiency, with a maximal efficiency of 83.38% after 40 min, which is maintained until 50 min. However, a minor decrease in efficiency is induced by surpassing the dosage of the $CaFe_2O_4$ nanocatalyst.

The $CaFe_2O_4$ nanocatalyst substantially enhanced the treatment efficiency of AOII from aqueous solution and processed 83.38% of the TOC in 40 min with $CaFe_2O_4/O_3$ systems. At the same time, the TOC processing efficacy with O_3 alone was only 58%. A synergistic combination of the gas phase (O_3), liquid phase (AOII solution), and solid phase ($CaFe_2O_4$ nanocatalyst)

© 2023 The Author(s). Published by the Royal Society of Chemistry

Open Access Article. Published on 02 October 2023. Downloaded on 2/9/2026 11:33:56 AM.
This article is licensed under a Creative Commons Attribution-NonCommercial 3.0 Unported Licence.

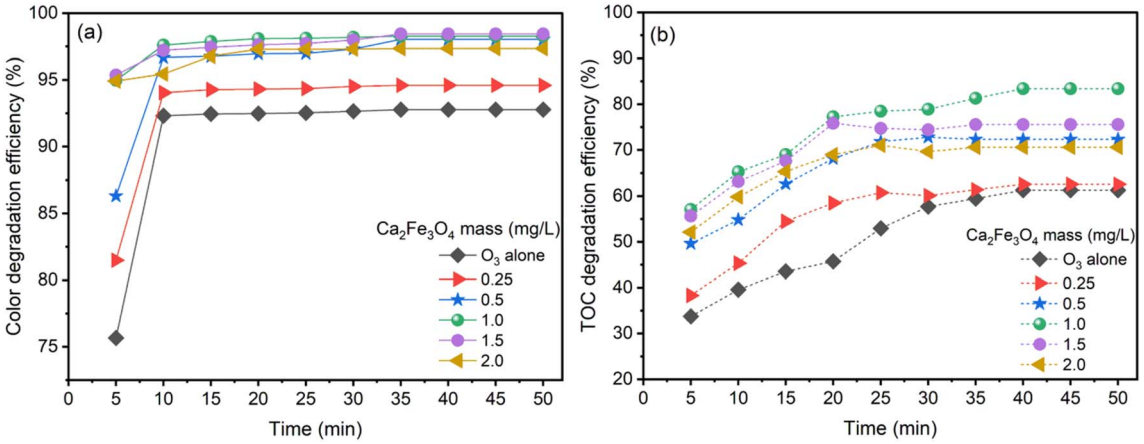

Fig. 4 Color and TOC degradation efficiency by $CaFe_2O_4$ nanoparticle catalytic ozonation (a and b) at various dosages of $CaFe_2O_4$. Conditions: [AOII] = 200 mg L^{-1}, initial pH = 9, contact time = 50 min, and reaction temperature = 25 ± 2 °C.

occurred when the $CaFe_2O_4$ nanocatalyst was introduced into the reactor in the presence of ozone (O_3).[26] This configuration allowed for the simultaneous interaction of O_3 and the azo dye (AOII) on the nanocatalyst's surface. Direct interactions between O_3 molecules and AOII resulted in the oxidation of AOII. Moreover, the $^{\bullet}OH$ radicals generated by catalytic ozonation processes contributed to the oxidation of AOII.

The $CaFe_2O_4$ nanocatalyst was indispensable to the system. First, it acted as an adsorbent, facilitating contact between the reactants and enhancing the overall process efficacy. It also provided sites where O_3 and $^{\bullet}OH$ radicals could react with AOII molecules, thereby enabling their oxidation. This cooperative action of the nanocatalyst, O_3, and $^{\bullet}OH$ radicals effectively removed color from the azo dye solution. There are also several plausible explanations for why the $CaFe_2O_4/O_3$ system was able to process a higher percentage of TOC than O_3 alone: (1) synergistic effect: the combination of the $CaFe_2O_4$ nanocatalyst and O_3 may have a synergistic effect in which the two components enhance the treatment efficacy of AOII. This may result from $CaFe_2O_4$'s ability to function as a catalyst to promote the decomposition of AOII by O_3 alone. The $CaFe_2O_4$ nanocatalyst has a high surface area, which can provide more active sites for the AOII and O_3 reactions. This can increase the reaction rate and enhance the treatment's efficacy. This may explain why $CaFe_2O_4/O_3$ could metabolize a more significant percentage of TOC than O_3 alone. However, it is essential to evaluate the optimal $CaFe_2O_4$ nanocatalyst dosage. Exceeding the optimal dosage may result in an inhibitory effect, reducing the decolorization and total organic carbon (TOC) removal effectiveness. Several factors can explain this phenomenon. For instance, an excessive quantity of the nanocatalyst may lead to the saturation of active sites on its surface, thereby reducing the availability of reactive sites for O_3 and $^{\bullet}OH$ radicals. In addition, at higher concentrations, the nanocatalyst may promote unintended side reactions, thereby reducing the efficiency of AOII oxidation and TOC removal.

According to previous investigations, an ozone (O_3) catalyst can be more effective at degrading azo dyes than O_3 alone. Using a catalyst in conjunction with ozone, catalytic ozonation is effective for degrading azo dyes. For instance, a study discovered that combining ozone and ZnO catalysts effectively degraded azo dyes.[53] According to another study, using a Ni-containing layered double hydroxide nanocatalyst in conjunction with ozone effectively degrades an azo dye.[54] The presence of Au/TiO_2 increased the corona discharge's sterilization efficiency from 73% to 91%. It decreased the O_3 concentration from 0.38 ppm to 0.04 ppm, whereas the presence of TiO_2 decreased the sterilization efficiency and O_3 concentration to 66% and 0.17 ppm, respectively.[55]

The effect of initial AOII concentration

Exhaustive experiments were conducted under tightly regulated conditions to evaluate the efficacy of the heterogeneous catalytic ozonation process ($CaFe_2O_4/O_3$ system) for varying concentrations of AOII. Experiments were conducted at pH 9, ambient temperature (26 ± 2 °C), and a discharge rate of 3.038 g h^{-1}. Adjusting the initial AOII concentration within the range of 100 to 500 mg L^{-1} corresponding to TOC concentrations ranging from 16.89 to 82.94 mg L^{-1} was required for the ozonation process. Fig. 5 depicts the effect of the initial AOII concentration on the removal of color and degradation graphically. As shown in Fig. 5, increasing the AOII concentration reduced the efficacy for color removal and TOC degradation, regardless of whether the $CaFe_2O_4/O_3$ system was used. When the AOII concentration was increased from 100 mg L^{-1} to 500 mg L^{-1}, a significant reduction in color was observed between 10 and 30 min later (Fig. 5a). When the AOII concentration increased from 100 to 500 mg L^{-1}, the TOC removal efficiency decreased from 85% to 62% (Fig. 5b). However, extending the treatment duration did not result in a significant improvement in TOC removal efficiency. Previous studies have also demonstrated that the efficiency of azo dye degradation by nano-catalyzed ozone decreases as the initial concentration of azo dyes increases.[56] Lowering the concentration of azo dyes, utilizing extreme pH conditions, and employing higher ozone concentrations have been identified as more advantageous for

Open Access Article. Published on 02 October 2023. Downloaded on 2/9/2026 11:33:56 AM.
This article is licensed under a Creative Commons Attribution-NonCommercial 3.0 Unported Licence.

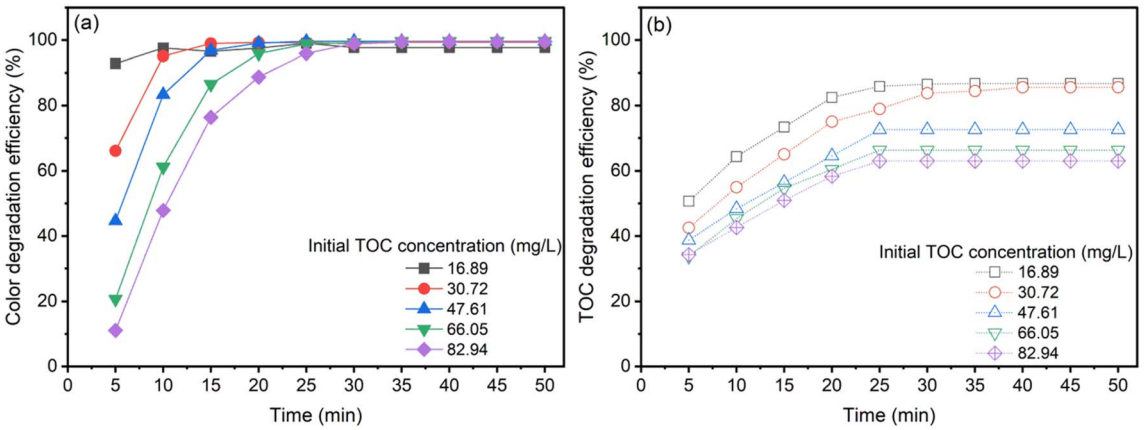

Fig. 5 The effect of AOII concentration on color (a) and TOC (b) degradation by $CaFe_2O_4$ nanoparticle catalytic ozonation processes. Conditions: $CaFe_2O_4$ dosage = 1.0 g, initial pH = 9, contact time = 50 min, and reaction temperature = 25 ± 2 °C.

dye degradation.[15] In addition, as previously mentioned, adding iron oxide as a catalyst does not result in a substantial reaction acceleration. Another study focusing on the degradation of acid red 18 dye using ZnO immobilized on a stone surface as a catalyst reveals a decrease in the rate constant as the initial dye concentration increases.[57]

The relative distribution of O_3, $CaFe_2O_4$ nanocatalyst, and $^{\bullet}OH$ radicals is significantly influenced by the concentration of AOII in the solution. With an increase in AOII concentration, the proportion of O_3, nanocatalyst, and $^{\bullet}OH$ radicals decreased compared to AOII. This observation revealed that as the concentration of AOII increased, the concentration of $^{\bullet}OH$ radicals remained unchanged. This phenomenon can be attributed to more AOII molecules occupying active sites on the catalyst's surface, inhibiting the production of $^{\bullet}OH$ radicals.[58] The occupation of active sites by AOII ions inhibited the production of $^{\bullet}OH$ radicals on the catalyst's surface, reducing their availability for degradation. The degradation efficiency of azo dyes also decreased due to the consumption of hydroxyl radicals by higher concentrations of organic dyes while the concentration of the oxidizing agent remained constant.[59] This observation illuminates the complexities of the catalytic ozonation process and highlights the importance of contemplating concentration-dependent phenomena for efficient pollutant removal.

Reaction rate constant and mechanism in AOII degradation by catalytic ozonation processes

Considering a distinct first-order reaction, the degradation rate is proportional to the removal of TOC.[26] In this regard, the following equation can be used to describe the kinetics of the reaction:

$$\mathrm{Ln}\,\frac{C}{C_0} = -Kt$$

Here, C_0 and C represent the concentration of AOII in the aqueous solution at the start of the reaction and after t min, respectively. The data align with a straight line when $\ln(C/C_0)$ is plotted against time, and k (the first-order rate constant) corresponds to the slope of this line. The rate constant was calculated by plotting $\ln(C/C_0)$ against time (t). With a coefficient of determination (R^2) ranging from 0.95 to 0.99, the linearity of these graphs validates the pseudo-first-order kinetics of the degradation process.

Fig. 6 and 7 illustrate the findings of plotting $\ln(C/C_0)$ against time (t) and calculating k values. In determining the reaction kinetics for TOC degradation by $CaFe_2O_4/O_3$ systems, the logarithmic transformation of the C/C_0 ratio against time is commonly employed. The determined rate constant, k, is consistent with a pseudo-first-order reaction. Fig. 6 depicts the influence of pH on k values, indicating that the degradation rate of TOC increased with increasing pH from 3 to 9 and then reduced slightly as the pH rose to 11. The k values for the O_3 alone system in AOII degradation ranged from 0.0146 min^{-1} to 0.017 min^{-1} as the pH of the solution increased from 3 to 9 and then decreased slightly to 0.0162 min^{-1} at pH 11 (Fig. 6a and c). As the pH of the AOII solution increased from 3 to 9, the k values for the $CaFe_2O_4/O_3$ system increased from 0.025 min^{-1} to 0.0311 min^{-1} and then decreased to 0.0302 min^{-1} at pH 11 (Fig. 6b and d). The obtained reaction rate constants correspond to the TOC degradation efficiency influenced by the AOII solution's pH. In addition, the results indicate that the k values for the $CaFe_2O_4/O_3$ system are substantially greater than those for O_3 alone. At a solution pH of 9, the k value for the $CaFe_2O_4/O_3$ system is 1.83 times that of O_3 alone. This further demonstrates that the $CaFe_2O_4$ nanocatalyst significantly enhanced the ozone degradation process of AOII. Except for the pH 5 condition in the $CaFe_2O_4/O_3$ system, where the R^2 value reached 0.927, most R^2 values fall between 0.9649 and 0.9959. Most treatment experiments exhibit linearity and are consistent with the pseudo-first-order kinetics of the degradation process, as indicated by the results.

Similarly to the pH effect, the plot of $\ln(C/C_0)$ and the reaction rate constant of TOC degradation using the $CaFe_2O_4/O_3$ system exhibits an increase in k values from 0.015 min^{-1} to 0.0361 min^{-1} when the amount of $CaFe_2O_4$ increased from 0.025 g L^{-1} to 1.0 g L^{-1}, followed by a decrease to 0.031 min^{-1}

© 2023 The Author(s). Published by the Royal Society of Chemistry

Open Access Article. Published on 02 October 2023. Downloaded on 2/9/2026 11:33:56 AM.
This article is licensed under a Creative Commons Attribution-NonCommercial 3.0 Unported Licence.

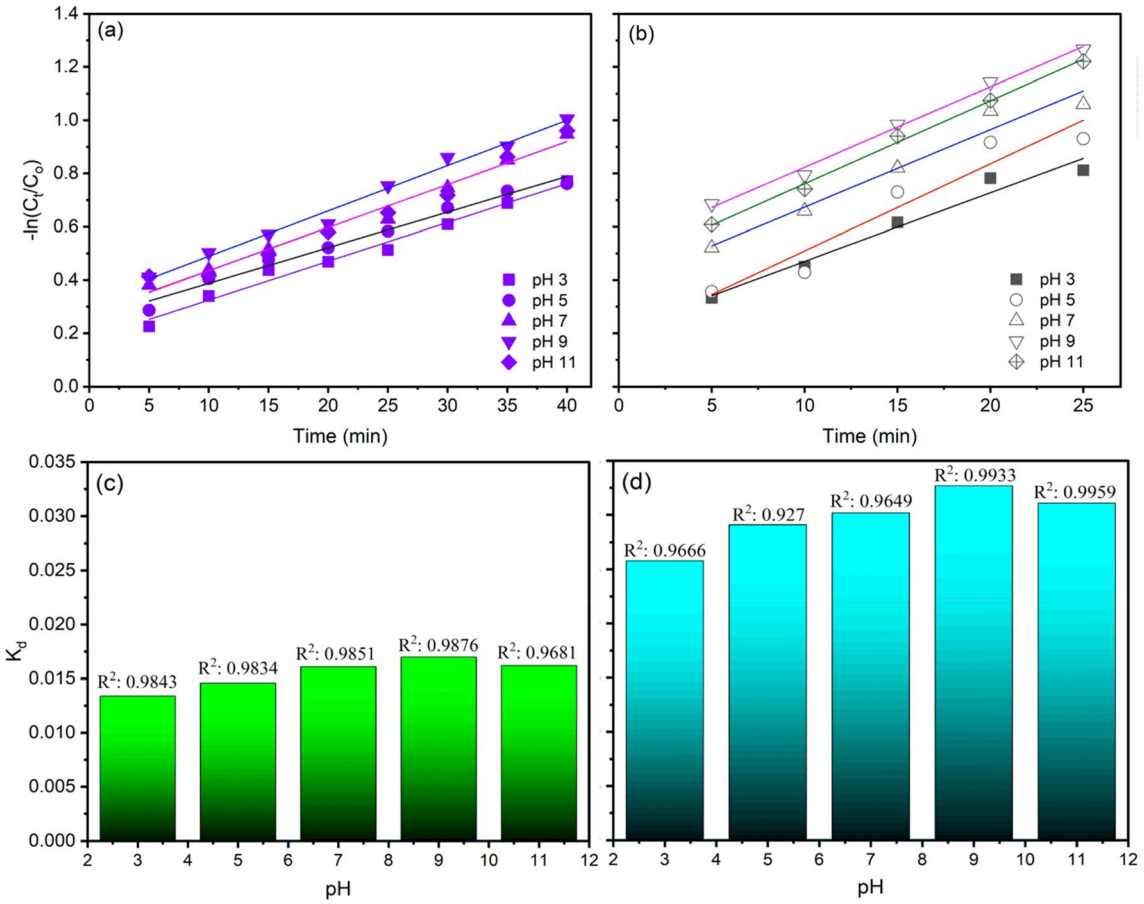

Fig. 6 The plots of $\ln(C/C_0)$ and reaction rate constant of TOC degradation by ozone alone (a and c) and $CaFe_2O_4$ nanoparticle catalytic ozonation processes (b and d) at various solution pH values.

and 0.0253 min^{-1} when the amount of $CaFe_2O_4$ was further increased to 1.5 and 2.0 g L^{-1} (Fig. 7a and c). The R^2 values were more significant than 0.95, except for the condition containing 1.5 g per L $CaFe_2O_4$. Fig. 7b and d illustrate a decreasing trend in the reaction rate constant (k) from 0.0643 min^{-1} to 0.0294 min^{-1} as the AOII concentration increased from 100 mg L^{-1} to 500 mg L^{-1}, which corresponds to TOC concentrations from 16.89 mg L^{-1} to 82.94 mg L^{-1}. The R^2 values for the conditions evaluating the effect of AOII concentration on TOC removal efficiency using the $CaFe_2O_4/O_3$ system were also greater than 0.99. The k values calculated correspond to the TOC treatment efficacy of the $CaFe_2O_4/O_3$ system when the $CaFe_2O_4$ and AOII concentrations were varied. These findings reaffirm the applicability of the reaction rate constant (k) according to a pseudo-first-order equation and by the treatment model.

According to numerous investigations, most treatment experiments are linear and consistent with the pseudo-first-order kinetics of the degradation process. According to Olea-Mejia *et al.*,[60] Fe nanoparticles can substantially accelerate the degradation of phenolphthalein. The degree of phenolphthalein mineralization was also determined by measuring the total organic carbon (TOC) concentration. Brito *et al.*[61] demonstrated that using a continuous reactor for the catalytic ozonation process and devising a kinetic model can provide the required technical data to support the scaling up of the process for the degradation of organic carbon in landfill leachate. Franco *et al.*[62] reported that the degradation rate of textile dyes evaluated by total organic carbon is substantially more influenced by pH and ozone exposure time than by dye composition.

Several stages compose the mechanism of AOII degradation by the $CaFe_2O_4$ nanocatalytic ozone process (Fig. 8). The initial phase was absorption: the $CaFe_2O_4$ nanocatalyst has a high affinity for organic molecules and a large surface area (379 m^2 g^{-1}). This nanocatalyst's high surface area was ascribed to its small size, which was typically on the order of tens of nanometers. This compact size increases the number of sites on the surface that can interact with reactant molecules, resulting in more significant activity. The subsequent step was ozone activation: ozone (O_3) is introduced into the system and activated in the presence of the $CaFe_2O_4$ nanocatalyst. The catalyst's surface contains active sites where ozone molecules can endure partial decomposition to form reactive oxygen species, such as hydroxyl radicals ($^{\bullet}OH$) and superoxide radicals ($^{\bullet}O_2^-$). Phase three was the production of reactive species: the activated ozone and reactive species generated from the catalyst surface, such as $^{\bullet}OH$ and $^{\bullet}O_2^-$,[63] were essential for the degradation of AOII. These highly reactive species attacked the adsorbed AOII

Open Access Article. Published on 02 October 2023. Downloaded on 2/9/2026 11:33:56 AM.
This article is licensed under a Creative Commons Attribution-NonCommercial 3.0 Unported Licence.

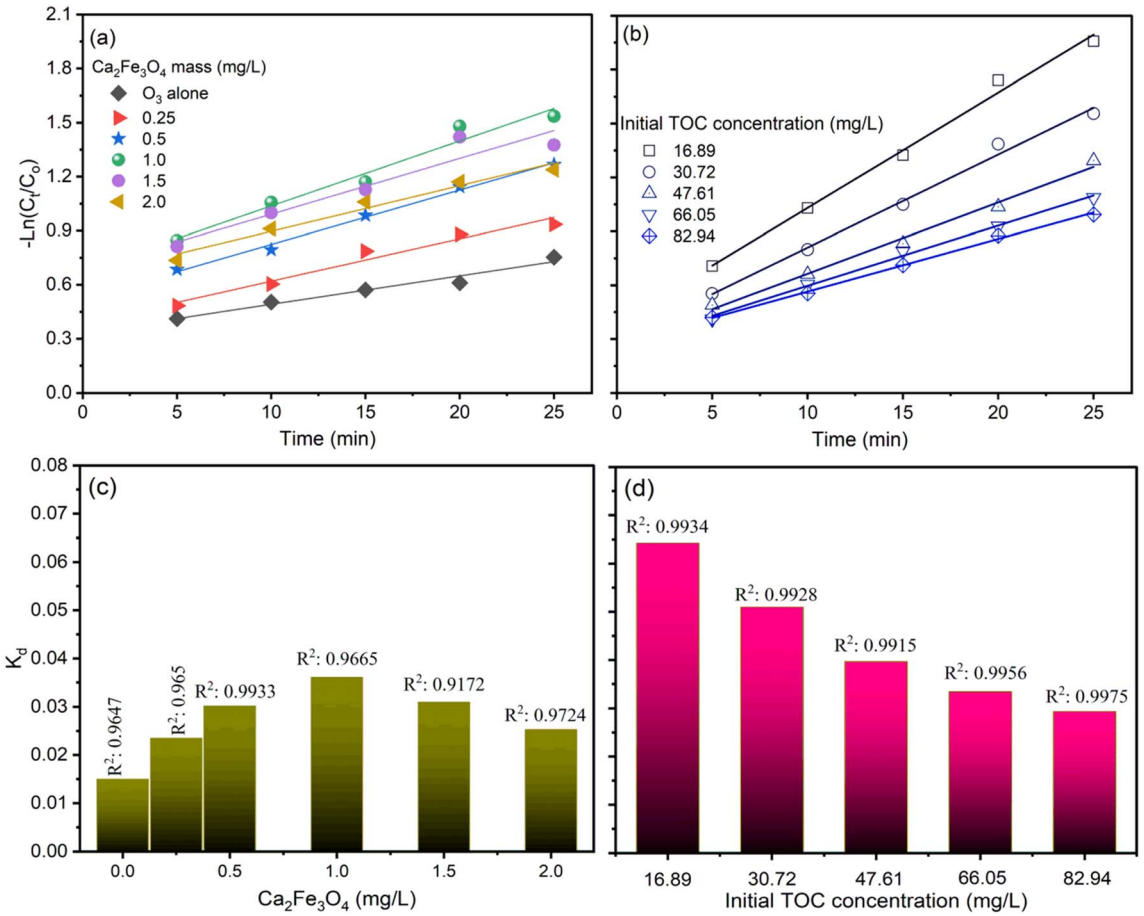

Fig. 7 The plots of $\ln(C/C_0)$ and reaction rate constant of TOC degradation by $CaFe_2O_4$ nanoparticle catalytic ozonation processes at various amounts of $CaFe_2O_4$ (a and c) and AOII concentration (b and d).

molecules, causing chemical bonds to dissolve and the dye to degrade. Phase 4 consists of degrading reactions: various chemical reactions, including oxidation, hydroxylation, and azo bond cleavage,[31] contribute to the degradation of AOII. The reactive species attacked the molecular structure of AOII, resulting in the formation of organic compounds that are smaller and less complex. These degradation products are frequently less environmentally harmful than the original pigment molecule. As the degradation reactions proceed, the degraded molecules desorb from the catalyst's surface, allowing

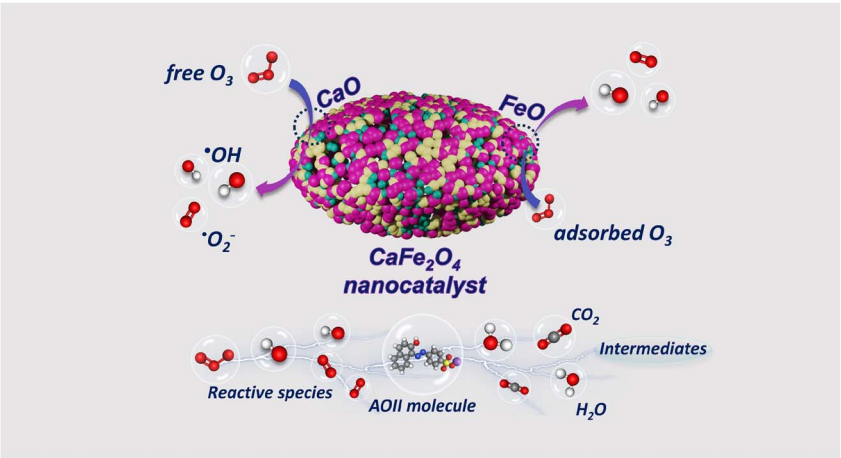

Fig. 8 Schematic diagram of the degradation mechanism of AOII using the $CaFe_2O_4$ nanocatalyst.

© 2023 The Author(s). Published by the Royal Society of Chemistry

Open Access Article. Published on 02 October 2023. Downloaded on 2/9/2026 11:33:56 AM.
This article is licensed under a Creative Commons Attribution-NonCommercial 3.0 Unported Licence.

new AOII molecules to adsorb and continue the degradation process. In subsequent reactions, such as mineralization, the degradation products are transformed into simpler inorganic compounds, such as carbon dioxide (CO_2), water (H_2O), and intangible ions.[64]

The $CaFe_2O_4$ nanocatalyst, composed of CaO and FeO, exhibits dual functionality as an adsorption and heterogeneous catalyst in ozone oxidation reactions. The material analysis results from EDX, XRD, and FTIR data (Fig. 2) confirm the presence of CaO and FeO on the surface of the nano $CaFe_2O_4$ nanocatalyst during the ozonation processes, which enhances the decomposition of O_3 and leads to the generation of $^{\bullet}OH$ radicals. The $CaFe_2O_4$ nanocatalyst provides active sites on its surface, allowing for the participation of both the catalyst and $^{\bullet}OH$ radicals in the ozone oxidation reaction for the degradation of AOII. The responses that predominantly yield $^{\bullet}OH$ radicals in the ozonation processes follow three mechanisms: H atom abstraction, $^{\bullet}OH$ addition to C=C, and $^{\bullet}OH$ interaction with S and N atoms from AOII. The $CaFe_2O_4$ nanocatalyst, with its CaO and FeO structure, plays a crucial role in efficiently adsorbing O_3 and surface pollutants, thereby accelerating the O_3 decomposition process and increasing the production of hydroxyl ($^{\bullet}OH$) radicals, which are essential for the degradation of AOII. The fragmentation of AOII through the intervention of $^{\bullet}OH$ radicals is achieved through the heterogeneous catalysis mechanism inherent in the ozone oxidation process. The $CaFe_2O_4$ nanocatalyst, with its CaO and FeO composition, contributes to the catalytic performance of the catalyst in the ozone oxidation process. The activities of FeO and CaO are essential factors in the catalytic activity of the $CaFe_2O_4$ nanocatalyst. Previous studies showed that the Co^{2+}–HCO_3^- system can efficiently degrade the cationic dye methylene blue (MB).[65] However, when both AOII and MB are present in the solution, most of the Co^{2+} ions will form stable complexes with AOII, hindering the degradation of MB. The application of heterogeneous catalytic ozonation, such as using catalysts like alumina, has been explored for treating refractory organics in wastewater.[66] This demonstrates the broader application of stimuli in the degradation of organic compounds, similar to the role of the $CaFe_2O_4$ nanocatalyst in the ozonation processes.

Comparing azo dye degradation using heterogeneous ozonation processes

Table 1 presents the AOII removal capacity comparison of the $CaFe_2O_4/O_3$ system with other systems. Among the studies highlighted, the utilization of nano $CaFe_2O_4$ as the catalyst in conjunction with ozone for AOII degradation was undertaken in our ongoing research. The optimized parameters included maintaining a pH of 9, applying a catalyst dosage of 1.0 g per L $CaFe_2O_4$ nanocatalyst, and varying AOII initial concentrations from 100 to 500 mg L^{-1}. This configuration resulted in the attainment of a substantial 85% efficiency in the removal of TOC. Notably, the study demonstrated significant prowess in the degradation of AOII.

The current study observed a significant efficiency enhancement compared to Hassani *et al.*'s (2019)[54] findings for employing dual-layered nickel hydroxide (Ni-LDH) to degrade methyl orange. This improvement became particularly evident when contrasted with the reported 72% COD removal efficiency. The discoveries in this investigation also demonstrate superior effectiveness compared to the removal efficacy of active brilliant red X-3B using ozonation catalyzed by the natural mineral brucite, as conducted by Dong *et al.* (2007),[67] achieving a COD degradation efficiency of 32% under experimental conditions of pH 9.24, catalyst dosage of 0.5 g L^{-1}, active brilliant red X-3B concentration of 500 mg L^{-1} and a reaction time of 30 min (Table 1).

In the context of Shokrollahzadeh *et al.* (2019)[17] research concerning nano-ZnO/pearl stone use for reactive blue 5 degradation, a higher efficacy was demonstrated, surpassing the 92% TOC removal efficiency. Compared to Zhang *et al.* (2022),[68] who focused on methyl orange degradation by utilizing nano MnO_2 particles, the current study showed slightly lower degradation efficiency. This is emphasized by the outstanding removal efficiency of 98.37% for methyl orange. Similarly, in contrast to the results of Bagheri *et al.* (2021),[69] where Fe_2O_3/MoS_2 nanocomposites were employed for acid blue 113 degradation, achieving a removal efficiency of 99.0%, our study exhibited slightly lower efficacy. Similarly, compared to Van *et al.* (2019),[26] targeting reactive red 24 degradation through iron slag, the present study showed similar effectiveness. This achievement corresponds to a COD removal efficiency of 84%.

Reusability of the catalyst

The significant role of wastewater removal applications, encompassing general and specific instances such as textile dye effluent, is underscored by the vital importance of stability and reusability exhibited by the $CaFe_2O_4$ nanocatalyst in the catalytic ozonation processes. Consequently, after each reaction cycle, the solid residue underwent collection *via* filtration and thorough rinsing with distilled water and was subjected to drying at 80 °C for 12 h. This treated residue was redeployed in consecutive cycles to evaluate its stability and reusability. The experimental conditions entailed maintaining the pH of 9, utilizing the catalyst dosage of 1 g L^{-1}, applying the initial AOII concentration of 200 mg L^{-1}, and employing the reaction time of 40 min. Fig. 9 presents the results thus obtained. The findings illustrate insubstantial fluctuations in AOII degradation across five successive operations. The efficiency of AOII degradation experienced a slight reduction from 85% to 69% after five consecutive cycles, indicating the non-significant degradation of the nano $CaFe_2O_4$ catalyst during the ozonation process and the continual preservation of its notable stability. The diminished catalytic effectiveness of the $CaF_{e2}O_4/O_3$ system potentially stems from catalyst attrition during the reusability experiments, aligning with prior research findings. Nguyen *et al.* (2023)[71] documented a decline in treatment efficacy throughout five consecutive runs while employing a biochar-supported $NiFe_2O_4$ composite as a catalyst for the ozone/Fenton treatment of moxifloxacin in wastewater. Another study also revealed that the efficacy of the cyclic hydrothermal conversion of ethyl levulinate (EL) into γ-valerolactone (GVL),

Open Access Article. Published on 02 October 2023. Downloaded on 2/9/2026 11:33:56 AM. This article is licensed under a Creative Commons Attribution-NonCommercial 3.0 Unported Licence.

Table 1 Comparing the degradation of azo dyes through heterogeneous ozonation processes using different catalysts

Dyes	Catalyst	Optimal processing conditions	Degradation efficiency	References
AOII	$CaFe_2O_4$ nanoparticles	pH 9, $CaFe_2O_4$: 1.0 g L^{-1}, AOII concentration: 100–500 mg L^{-1}	85% TOC removal	This study
Methyl orange	Ni-based layered double hydroxides (Ni-LDHs) nanomaterials	Reaction time: 60 min, pH 9; ozone flow rate: 109 mg h^{-1}; catalyst dosage: 1 g L^{-1}; initial COD: 620 mg L^{-1}	72% COD removal	54
Methyl orange	MnO_2 nanoparticles	Initial pH 5.8, reaction time: 60 min, methyl orange concentration: 90 mg L^{-1}, catalyst dosage: 20 mg L^{-1}	98.37% methyl orange removal	68
AOII	ZnO nanoparticles	pH range: 4.6–9.6, ZnO nanoparticle: 1.0 g L^{-1}, AOII: 50–200 mg L^{-1}	90% TOC removal	70
Acid blue 113	Fe_2O_3/MoS_2 nanocomposite	Initial pH 6.4, nanocomposite: 20 mg, ozone flow: 0.2 g L^{-1} h^{-1}, and reaction time: 45 min	99.0% AOII removal	69
Reactive blue 5	Nano-ZnO/perlite	pH 11, reaction time: 60 min, dye concentration: 100 mg L^{-1}, initial TOC: 31.45 mg L^{-1}, catalyst dosage: 12 mg L^{-1}	92% TOC removal	17
Reactive red 24	Iron slag	pH 11, catalyst dosage: 1.5 g L^{-1}, initial reactive red 24 concentration: 300 mg L^{-1}, inlet O_3: 3.038 g h^{-1}, H_2O_2 concentration: 100 mg L^{-1}, reaction time: 40 min	84% COD removal	26
Active brilliant red X-3B	Natural mineral brucite	pH 9.24, catalyst dosage: 0.5 g L^{-1}, active brilliant red X-3B: 500 mg L^{-1}, reaction time: 30 min	32% COD removal	67

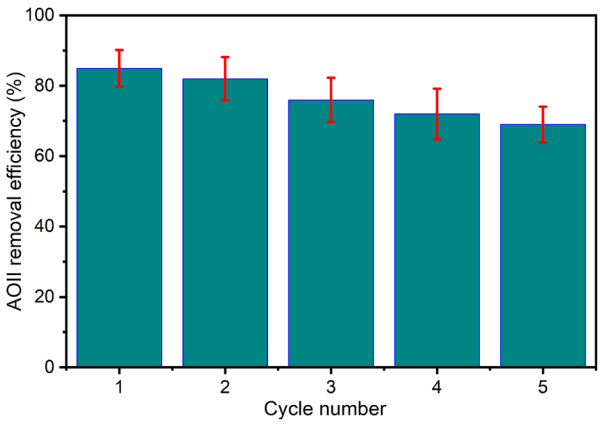

Fig. 9 Reusability of $CaFe_2O_4$ nanoparticles for catalytic ozonation processes at solution pH 9, the catalyst dosage of 1.0 g L^{-1}, initial AOII concentration of 200 mg L^{-1}, reaction time of 40 min and temperature of 25 ± 2 °C.

utilizing a layered O_v-WO_3@CB catalyst, exhibited a marginal decline from 98% to 91% after undergoing five recycling cycles, thereby emphasizing the intricate nature of catalytic responses over repeated operations.[72] The results indicated that the $CaFe_2O_4$ nanocatalyst could potentially eliminate azo dyes from wastewater.

Conclusion

This study investigated the degradation of AOII *via* the $CaFe_2O_4$ nanocatalytic ozonation approach. Experimental results revealed the factors affecting AOII degradation efficiency and kinetics. O_3 alone and $CaFe_2O_4/O_3$ systems remove AOII color nearly perfectly in experiments. Degradation was found to depend on the solution pH. The degradation of AOII increased with pH 3 to 9, while pH 11 slightly decreased it. AOII concentration also affected the degradation efficiency. AOII degradation was also examined with $CaFe_2O_4$ nanocatalyst mass. The main catalyst portion was crucial to degradation, according to the results. As the amount of the nanocatalyst increased from 0.025 g L^{-1} to 1.0 g L^{-1}, k values increased from 0.015 min^{-1} to 0.0361 min^{-1}. However, increasing the amount of the catalyst to 1.5 and 2.0 g L^{-1} decreased the reaction rate constant to 0.031 min^{-1} and 0.0253 min^{-1}, respectively. The findings also indicate that the efficiency of TOC removal decreased from 85% to 62% as the initial concentration of AOII increased from 100

© 2023 The Author(s). Published by the Royal Society of Chemistry

Open Access Article. Published on 02 October 2023. Downloaded on 2/9/2026 11:33:56 AM. This article is licensed under a Creative Commons Attribution-NonCommercial 3.0 Unported Licence.

to 500 mg L^{-1}. Determining the reaction rate constant confirmed pseudo-first-order degradation kinetics. At pH 9, the rate constant (k) of the $CaFe_2O_4/O_3$ system ranged from 0.025 min^{-1} to 0.0311 min^{-1}, depending on catalyst quantity. Ozone alone had a rate constant of 0.0146 min^{-1} to 0.017 min^{-1} at the same pH. These results show that the $CaFe_2O_4$ nanocatalytic ozonation degrades AOII. Degradation efficiency and rate depended on pH, AOII concentration, and catalyst dosage. $CaFe_2O_4$ nanoparticles catalyzed degradation faster than ozone alone. The $CaFe_2O_4/O_3$ system outperformed ozone at pH 9. The $CaFe_2O_4$ nanocatalytic ozonation process can remediate wastewater containing AOII and other azo dyes. Its use in water treatment and environmental remediation requires optimization and scaling-up research. This study illuminates catalytic ozonation kinetics and mechanisms and lays the groundwork for future research.

Data availability

The data that has been used is confidential.

Author contributions

Van Hung Hoang: conceptualization, methodology, software. Huu Tap Van: conceptualization, methodology, software. Huu Tap Van: data curation, writing – original draft. Thi Cuc Luu: data curation, writing – original draft. Thuy Linh Vi: visualization, investigation. Luong Thi Quynh Nga: visualization, investigation. Van Hung Hoang: supervision. Gio Serafin Ivan Jimenez Marcaida: conducted experiments, software, validation. Huu Tap Van: writing – review & editing. All authors provided critical feedback and helped shape the research, analysis, and manuscript.

Conflicts of interest

The authors declare that they have no known competing financial interests or personal relationships that could have appeared to influence the work reported in this paper.

Acknowledgements

This work was financially supported by the Vietnam Ministry of Education and Training under project number: B2022-TNA-45.

References

1 B. Lellis, C. Z. Fávaro-Polonio, J. A. Pamphile and J. C. Polonio, *Biotechnol. Res. Innov.*, 2019, **3**, 275–290.
2 T. Islam, M. R. Repon, T. Islam, Z. Sarwar and M. M. Rahman, *Environ. Sci. Pollut. Res. Int.*, 2023, **30**, 9207–9242.
3 R. Al-Tohamy, S. S. Ali, F. Li, K. M. Okasha, Y. A.-G. Mahmoud, T. Elsamahy, H. Jiao, Y. Fu and J. Sun, *Ecotoxicol. Environ. Saf.*, 2022, **231**, 113160.
4 K. S. Bharathi and S. T. Ramesh, *Appl. Water Sci.*, 2013, **3**, 773–790.
5 Y. Ning, Y. Yang, C. Wang, T. Ngai and Z. Tong, *Chem. Commun.*, 2013, **49**, 8761–8763.
6 T. A. Aragaw and F. M. Bogale, *Front. Environ. Sci.*, 2021, **9**, 764958.
7 P. De Luca, P. Foglia, C. Siciliano, J. B. Nagy and A. Macario, *Environments*, 2019, **6**, 101–129.
8 J. I. Mary Jency, L. Gowrisankar, J. Krishnaveni and N. Renugadevi, *J. Environ. Treat. Tech.*, 2020, **9**, 218–223.
9 H. F. Liu, B. J. Zheng, A. Q. Dao, S. T. Yi, D. S. Jiang, C. Y. Fu and F. Xiao, *Mater. Res. Innovations*, 2014, **18**, S2-707–S2-710.
10 I. Gültekin and N. H. Ince, *Ultrason. Sonochem.*, 2006, **13**, 208–214.
11 M. H. Beak, C. O. Ijagbemi and D. S. Kim, *J. Environ. Sci. Health, Part A: Toxic/Hazard. Subst. Environ. Eng.*, 2009, **44**, 623–629.
12 A. Chaturvedi, B. N. Rai, R. S. Singh and R. P. Jaiswal, *Rev. Chem. Eng.*, 2022, **38**, 617–639.
13 M. Torun, D. Aracagök and M. Kabalak, *Hittite J. Sci. Eng.*, 2018, **5**, 307–311.
14 Z. Y. Bai, Q. Yang and J. L. Wang, *Int. J. Environ. Sci. Technol.*, 2016, **13**, 483–492.
15 C. A. T. Toro, J. L. A. Dagostin, É. de Castro Vasques, M. R. Spier, L. Igarashi-Mafra and T. L. P. Dantas, *Can. J. Chem. Eng.*, 2020, **98**, 2530–2544.
16 Q. Dai, Z. Zhang, T. Zhan, Z.-T. Hu and J. Chen, *ACS Omega*, 2018, **3**, 6506–6512.
17 S. Shokrollahzadeh, M. Abassi and M. Ranjbar, *Environ. Eng. Res.*, 2019, **24**, 513–520.
18 A. D. Bokare, R. C. Chikate, C. V. Rode and K. M. Paknikar, *Environ. Sci. Technol.*, 2007, **41**, 7437–7443.
19 Y. Meng, S. Yang and H. Li, *ChemSusChem*, 2022, **15**, e202102581.
20 H. Li, Z. Fang, R. L. Smith and S. Yang, *Prog. Energy Combust. Sci.*, 2016, **55**, 98–194.
21 S. Zhang, H. Ren, K. Fu, W. Cheng, D. Wu, C. Luo, S. Jiang, J. Li and M. Zhang, *Front. Energy Res.*, 2022, **9**, 1–8.
22 R. Rajesh, E. Sujanthi, S. S. Kumar and R. Venkatesan, *Phys. Chem. Chem. Phys.*, 2015, **17**, 11329–11340.
23 S. Krishna, P. Sathishkumar, N. Pugazhenthiran, K. Guesh, R. V. Mangalaraja, S. Kumaran, M. A. Gracia-Pinilla and S. Anandan, *RSC Adv.*, 2020, **10**, 16473–16480.
24 B. Rodríguez-Cabo, I. Rodríguez-Palmeiro, R. Corchero, R. Rodil, E. Rodil, A. Arce and A. Soto, *Water Sci. Technol.*, 2016, **75**, 128–140.
25 N. H. Sulaiman, M. J. Ghazali, J. Yunas, A. Rajabi, B. Y. Majlis and M. Razali, *Ceram. Int.*, 2018, **44**, 46–50.
26 H. T. Van, L. H. Nguyen, T. K. Hoang, T. P. Tran, T. A. Vo, T. T. Pham and X. C. Nguyen, *Sep. Purif. Technol.*, 2019, **224**, 431–442.
27 S. Alhassan, M. Alshammari, K. Alshammari, T. Alotaibi, A. H. Alshammari, Y. Fawaz, T. A. M. Taha and M. Henini, *Polymers*, 2023, **15**(9), 2223.
28 M. I. ur Rahman, H. M. Khan, M. N. Ashiq, M. U. Islam, S. A. Buzdar, I. Sadiq, S. Honey, Z. Batool, R. Sheikh, M. Zahid, M. A. Assiri, M. Imran and T. Alshahrani, *RSC Adv.*, 2023, **13**, 14461–14471.

© 2023 The Author(s). Published by the Royal Society of Chemistry

Open Access Article. Published on 02 October 2023. Downloaded on 2/9/2026 11:33:56 AM.
This article is licensed under a Creative Commons Attribution-NonCommercial 3.0 Unported Licence.

29 S. Altaf, H. Ajaz, M. Imran, A. Ul-Hamid, M. Naz, M. Aqeel, A. Shahzadi, A. Shahbaz and M. Ikram, *Appl. Nanosci.*, 2020, **10**, 2113–2127.
30 M. Goodarzi, S. Joukar, D. Ghanbari and K. Hedayati, *J. Mater. Sci.: Mater. Electron.*, 2017, **28**, 12823–12838.
31 M. M. Tauber, G. M. Guebitz and A. Rehorek, *Appl. Environ. Microbiol.*, 2005, **71**, 2600–2607.
32 F. J. Poblete, P. Corrochano and B. Cabañas, *J. Phys. Org. Chem.*, 2009, **22**, 546–549.
33 A. Lopez, H. Benbelkacem, J. -S. Pic and H. Debellefontaine, *Environ. Technol.*, 2004, **25**, 311–321.
34 M. Tokumura, T. Katoh, H. Ohata and Y. Kawase, *Ind. Eng. Chem. Res.*, 2009, **48**, 7965–7975.
35 E. J. Smutny, M. C. Caserio and J. D. Roberts, *J. Am. Chem. Soc.*, 1960, **82**, 1793–1801.
36 M. Harfenist, *J. Org. Chem.*, 1963, **28**, 1834–1837.
37 D. R. Corbin, W. S. Willis, E. N. Duesler and G. D. Stucky, *J. Am. Chem. Soc.*, 1980, **102**, 5969–5971.
38 J. Santrock, R. A. Gorski and J. F. O'Gara, *Chem. Res. Toxicol.*, 1992, **5**, 134–141.
39 C.-C. Wu, W.-J. Huang and B.-H. Ji, *J. Environ. Sci. Health, Part A: Toxic/Hazard. Subst. Environ. Eng.*, 2015, **50**, 1116–1126.
40 P. Van Aken, N. Lambert, R. den Broeck, J. Degrève and R. Dewil, *Environ. Sci.: Water Res. Technol.*, 2019, **5**, 444–481.
41 S. Khuntia, S. K. Majumder and P. Ghosh, *Ind. Eng. Chem. Res.*, 2013, **52**, 318–326.
42 R. Zhang, C. Zhang, X. Cheng, L. Wang, Y. Wu and Z. Guan, *J. Hazard. Mater.*, 2007, **142**, 105–110.
43 J. Kaushal, M. Khatri and S. K. Arya, *Clean. Eng. Technol.*, 2021, **2**, 100083.
44 Y. Ma, L. Sun, R. Wang, Y. Gu, H. Xu and P. Lei, *Molecules*, 2022, **27**(21), 7209.
45 J. Roussy, M. Van Vooren and E. Guibal, *J. Appl. Polym. Sci.*, 2005, **98**, 2070–2079.
46 J. T. Marois-Fise, A. Carabin, A. Lavoie and C. C. Dorea, *Appl. Environ. Microbiol.*, 2013, **79**, 2107–2109.
47 M. Zhang, Q. Yao, W. Guan, C. Lu and J.-M. Lin, *J. Phys. Chem. C*, 2014, **118**, 10441–10447.
48 *Advanced Ozonation Processes for Water and Wastewater Treatment: Active Catalysts and Combined Technologies*, ed. H. Cao, Y. Xie, Y. Wang and J. Xiao, The Royal Society of Chemistry, 2022.
49 X. Li, L. Fu, F. Chen, S. Zhao, J. Zhu and C. Yin, *Catalysts*, 2023, **13**(2), 342.
50 J. S. Park, H. Choi and K. H. Ahn, *Water Sci. Technol.*, 2003, **47**, 179–184.
51 Y. Yuan, M. Mortazavi, S. Garg, J. Ma and T. D. Waite, *ACS ES&T Engg*, 2022, **2**, 210–221.
52 Y. Wang, L. Gai, W. Ma, H. Jiang, X. Peng and L.-C. Zhao, *Ind. Eng. Chem. Res.*, 2015, **54**, 2279–2289.
53 R. B. Pachwarya, E. N. Hidayah, R. Kashyap, A. Ramanathan, R. S. Meena, P. K. Meena and S. Q. Z. Nisa, *International Journal of Eco-Innovation in Science and Engineering*, 2022, **1**, 41–44.
54 K. El Hassani, D. Kalnina, M. Turks, B. H. Beakou and A. Anouar, *Sep. Purif. Technol.*, 2019, **210**, 764–774.
55 B. Zhu, Q. Li, Y. Gao, Y. Yan, Y. Zhu and L. Xu, *Plasma Sci. Technol.*, 2022, **25**, 15505.
56 S. Liakou, S. Pavlou and G. Lyberatos, *Water Sci. Technol.*, 1997, **35**(4), 279–286.
57 H. Mahdizadeh, A. Nasiri, M. A. Gharaghani and G. Yazdanpanah, *MethodsX*, 2020, **7**, 101118.
58 K. Okitsu, K. Iwasaki, Y. Yobiko, H. Bandow, R. Nishimura and Y. Maeda, *Ultrason. Sonochem.*, 2005, **12**, 255–262.
59 V. Vaiano and I. De Marco, *Separations*, 2023, **10**(4), 230.
60 O. Olea-Mejia, M. Fernández-Mondragón, C. Barrera-Díaz and A. Cabral-Prieto, *Int. J. Photoenergy*, 2017, 9314764.
61 R. P. de Brito, H. J. I. Filho, L. G. Aguiar, M. A. K. de Alcântara, A. A. G. Siqueira and P. C. M. Da Rós, *Ind. Eng. Chem. Res.*, 2019, **58**, 9855–9863.
62 D. V. Franco, W. F. Jardim, J. F. C. Boodts and L. M. Da Silva, *Clean: Soil, Air, Water*, 2008, **36**, 34–44.
63 G. Munuera, V. Rives-Arnau and A. Saucedo, *J. Chem. Soc., Faraday Trans. 1*, 1979, **75**, 736–747.
64 J. Wang and Z. Bai, *Chem. Eng. J.*, 2017, **312**, 79–98.
65 X. Long, Z. Yang, H. Wang, K. Peng, Q. Zeng and X. Aihua, *Ind. Eng. Chem. Res.*, 2012, **51**, 11998–12003.
66 B. Gao, H. Zhang, F. Wang, X. Xiong, K. Tian, Y. Sun and T. Yu, *Catalysts*, 2019, **9**, 241.
67 Y. Dong, K. He, B. Zhao, Y. Yin, L. Yin and A. Zhang, *Catal. Commun.*, 2007, **8**, 1599–1603.
68 X. Zhang, B. Zhou, S. Yin, Y. Wang, X. Zhang, Q. Meng, F. Meng, C. Wei and G. Wen, *Vacuum*, 2022, **206**, 111495.
69 F. Bagheri and N. Chaibakhsh, *Sep. Sci. Technol.*, 2021, **56**, 3022–3032.
70 J. Lu, X. Wei, Y. Chang, S. Tian and Y. Xiong, *J. Chem. Technol. Biotechnol.*, 2016, **91**, 985–993.
71 T. H. Nguyen, X. H. Nguyen, T. G. Do and L. H. Nguyen, *Chem. Eng. J. Adv.*, 2023, **16**, 100550.
72 Y. Meng, Y. Jian, J. Li, H. Wu, H. Zhang, S. Saravanamurugan, S. Yang and H. Li, *Chem. Eng. J.*, 2023, **452**, 139477.

© 2023 The Author(s). Published by the Royal Society of Chemistry